Received: 8 August 2023 | Revised: 4 October 2023 | Accepted: 4 October 2023

DOI: 10.1002/kin.21697

INTERNATIONAL JOURNAL OF CHEMICAL KINETICS WILEY

RESEARCH ARTICLE

Rate coefficients for the gas-phase OH + furan (C_4H_4O) reaction between 273 and 353 K

Maria E. Angelaki[1] | **Manolis N. Romanias**[2] | **James B. Burkholder**[3] | **Vassileios C. Papadimitriou**[1,3,4]

[1]Laboratory of Photochemistry and Chemical Kinetics, Department of Chemistry, University of Crete, Vassilika Vouton, Heraklion, Crete, Greece

[2]IMT Nord Europe, Institut Mines-Télécom, Univ. Lille, Centre for Energy and Environment, Lille, France

[3]Chemical Sciences Laboratory, National Oceanic and Atmospheric Administration, Boulder, Colorado, USA

[4]Cooperative Institute for Research in Environmental Sciences, University of Colorado, Boulder, Colorado, USA

Correspondence
Vassileios C. Papadimitriou, Laboratory of Photochemistry and Chemical Kinetics, Department of Chemistry, University of Crete, Vassilika Vouton, 70013, Heraklion, Crete, Greece.
Email: bpapadim@uoc.gr

Manolis N. Romanias, IMT Nord Europe, Institut Mines-Télécom, Univ. Lille, Centre for Energy and Environment, Lille F-59000, France.
Email: emmanouil.romanias@imt-nord-europe.fr

Abstract

Rate coefficients, k_1, for the gas-phase OH radical reaction with the heterocyclic ether C_4H_4O (1,4-epoxybuta-1,3-diene, furan) were measured over the temperature range 273–353 K at 760 Torr (syn. air). Experiments were performed using: (i) the photochemical smog chamber THALAMOS (thermally regulated atmospheric simulation chamber, IMT NE, Douai-France) equipped with Fourier Transform Infrared (FTIR) and Selected Ion Flow Tube Mass Spectrometry (SIFT-MS) detection methods and (ii) a photochemical reactor coupled with FTIR spectroscopy (PCR, University of Crete, Greece). k_1(273–353 K) was measured using a relative rate (RR) method, in which the loss of furan was measured relative to the loss of reference compounds with well-established OH reaction rate coefficients. k_1(273–353 K) was found to be well represented by the Arrhenius expression $(1.30 \pm 0.12) \times 10^{-11}$ exp[(336 ± 20)/T] cm^3 molecule^{-1} s^{-1}, with k_1(296 K) measured to be $(4.07 \pm 0.32) \times 10^{-11}$ cm^3 molecule^{-1} s^{-1}. The k_1 (296 K) and pre-exponential quoted error limits are 2σ and include estimated systematic errors in the reference rate coefficients. The observed negative temperature dependence is consistent with a reaction mechanism involving the OH radical association to a furan double bond. Quantum mechanical molecular calculations show that OH addition to the α-carbon (ΔH_r(296 K) = −121.5 kJ mol^{-1}) is thermochemically favored over the β-carbon (ΔH_r(296 K) = −52.9 kJ mol^{-1}) addition. The OH-furan adduct was found to be stable over the temperature range of the present measurements. Maleic anhydride ($C_4H_2O_3$) was identified as a minor reaction product, 3% lower-limit yield, demonstrating a non-ring-opening active reaction channel. The present results are critically compared with results from previous studies of the OH + furan reaction rate coefficient. The infrared spectrum of furan was measured as part of this study and its estimated climate metrics are reported.

KEYWORDS
atmospheric chemistry, biofuel, biomass burning, gas-phase kinetics, infrared spectra

1 | INTRODUCTION

Heterocyclic oxygenated volatile organic compounds (c-OVOCs) have been identified as gas-phase products of biomass burning (BB).[1,2] Furan (C_4H_4O, 1,4-epoxybuta-1,3-diene) is the base structural unit of furanoids, where the hydrogen in furan is substituted with functional groups such as hydroxy (-OH), aldehyde (-(H)C=O), ketone (-(R)C=O) and methyl (-CH_3). In spite of their importance, the c-OVOCs impact on air quality, human health,[3] and climate are not fully characterized.[4] c-OVOCs have also been proposed as renewable biofuels via the catalytic conversion of lignocellulosic biomass.[5]

There are limited studies of gas-phase furanoid kinetics, with most studies being performed at room temperature and atmospheric pressure. The kinetic study of reaction (1):

$$OH + C_4H_4O\,(furan) \rightarrow products \quad (1)$$

is expected to provide, in addition to information about furan atmospheric reactivity and its degradation mechanism, insights into the OH radical chemistry of the furanoid class of compounds.

There are several studies of k_1(298 K)[6–10] in the literature and two temperature dependent measurements[11,12] that have significant systematic discrepancies. Lee and Tang[6] were the first to report k_1(298 K) using a Flash Photolysis/Resonance Fluorescence technique (FP/RF). Atkinson et al.,[7] Tuazon et al.,[8,9] and Bierbach et al.[10] subsequently measured k_1(298 K) using RR methods. The results from these three studies are in good agreement with an average k_1(298 K) value of 4.04×10^{-11} cm^3 $molecule^{-1}$ s^{-1}, with a 7% (2 sigma) uncertainty. Wine and Thompson[12] reported k_1(254–425 K) using a FP/RF technique to have a negative temperature dependence. More recently, Whelan et al.[11] reported k_1(294–595 K) over a wide range of pressure, 5–200 mbar (N_2) and 2–10 bar (He); no pressure dependence was observed. The Whelan et al.[11] study, however, reported k_1(T) values that are systematically lower than previously reported values by 15%–20%. Therefore, detailed and accurate furan gas-phase reactivity is still desired to elucidate the atmospheric oxidation mechanism and to evaluate potential environmental and human health impacts.[13,14]

In the present study, rate coefficients for the OH radical + furan reaction, k_1(T), were measured between 273 and 353 K at atmospheric pressure by measuring the loss of furan relative to four different reference compounds. Kinetic measurements were carried out using the THALAMOS smog chamber (IMT NE, Douai, France) and the PCR apparatus (University of Crete–UoC, Greece). The thermochemistry of reaction 1 was calculated via quantum mechanical molecular calculations to evaluate the OH radical association site-specific reactivity. As part of this work, the infrared spectrum of furan was measured and used to derive its climate metrics. The present kinetic results are compared with the previous measurements described above and discrepancies in k_1(T) are discussed.

2 | EXPERIMENTAL DETAILS

In this section, experimental methods and setups used in this study are described. Two apparatuses were used to perform relative rate experiments: (a) The thermostated Teflon chamber "THALAMOS" (IMT NE) equipped with in-line FTIR spectroscopy and SIFT-MS was used to measure k_1(273–353 K) at 760 Torr (syn. air)[15,16] and (b) the photochemical reactor (PCR, UoC) coupled with FTIR spectroscopy[16–18] was used to measure k_1(296 K). Both apparatuses have been used in the past and only brief descriptions of the experimental setups and methods are given herein.[15–18]

2.1 | Chamber relative rate measurements: THALAMOS

THALAMOS consists of three main components, (i) a cuboid Teflon reactor, 0.6 m^3, housed in a climatic thermostatic cage (climatic box VT-4100, Vötsch industrietechnik, Germany) providing temperature regulation between 231 and 453 K, (ii) a set of 10 UV-A (PL-L 24 W/10/4P, Philips, Netherlands), and 10 UV-C (HNS-L 24 W 2G11, Osram, UK) photolysis lamps, equally spaced around the Teflon chamber inside the climatic box and (iii) FTIR and SIFT-MS detection setups.

Reactants, the OH radical precursor, H_2O_2, and bath gas were introduced into the chamber via independent inlets. The reaction mixture was allowed to mix inside the chamber utilizing four fans inside the chamber for a minimum of 20 min. Once reactants were well mixed, as verified via infrared and mass spectral signals, the UV-C lamps, maximum output at 254 nm, were turned on and the H_2O_2 photolysis led to OH radical formation, initiating the reaction. The reaction progress was monitored continuously via SIFT-MS (Voice 200 ultra, ~0.2 Hz sampling rate in most measurements) and FTIR (Antaris, Thermo).[19]

C_4H_4O loss was monitored relative to that of a selected reference compound. The concept in the RR method is that the reactant and a reference compound are lost solely via their reaction with the reactive species of interest, that is, the OH radical. Applying the rate law for the two reactants, it can be shown[20–22] that the rate coefficient of interest can

be obtained from the expression:

$$ln\frac{[C_4H_4O]_t}{[C_4H_4O]_0} = \frac{k_1}{k_{ref}} ln\frac{[Ref]_t}{[Ref]_0} \quad (3)$$

where $[C_4H_4O]$ and [Ref] are the C_4H_4O and reference concentrations and k_1 and k_{ref} are the OH rate coefficients for the furan and reference compound reactions, respectively. Possible first-order background losses, k_d, for furan and the reference compound, k'_d, can be accounted for, using:

$$\frac{1}{(t-t_0)}\ln\frac{[C_4H_4O]_{t_0}}{[C_4H_4O]_t} - k_d = \frac{k_1}{k_{ref}}\left[\frac{1}{(t-t_0)}\ln\frac{[Ref]_{t_0}}{[Ref]_t} - k'_d\right] \quad (4)$$

where t_0 is the irradiation start time. Control experiments were carried out at each temperature included in this study. k_d and reference compound k'_d were measured, with k_d being in the range (0.5–1.0) $\times 10^{-5}$ s^{-1}, while k'_d was negligible in all cases. Next, the reaction mixture was irradiated for ~2 h and photolysis loss of both furan and reference compound measured. Furan photolysis loss in THALAMOS (UV-C lamps) was measured to be $\sim 5 \times 10^{-6}$ s^{-1}, while in PCR (3rd harmonic of Nd:YAG laser, 355 nm) C_4H_4O photolysis loss was not measurable. Reference compound photolysis loss was also negligible, in both setups, under all experimental conditions. The sampling flow rate of SIFT-MS was ~25 cm^3 min^{-1}, which led to a change of less than 0.5% of the reaction volume over the duration of an experiment. The total background loss of furan during an actual kinetic experiment was always less than 4% of the OH kinetic loss.

Three reference compounds with well-established OH reaction rate coefficients were used in separate experiments: CH_2=C(CH_3)CH=CH_2 (isoprene), $k(T) = 3.00 \times 10^{-11} \exp(360/T)$, $k(296\ K) = 1.00 \times 10^{-10}$ cm^3 $molecule^{-1}$ s^{-1},[23] *n*-C_4H_9OH (*n*-butanol), $k(296\ K) = 0.85 \times 10^{-11}$ cm^3 $molecule^{-1}$ s^{-1},[24] and C_4H_8O (tetrahydrofuran, THF), $k(T) = 0.97 \times 10^{-11} \exp(177/T)$, $k(296\ K) = 1.76 \times 10^{-11}$ cm^3 $molecule^{-1}$ s^{-1}.[25]

The SIFT-MS detection system monitored the concentration of the reactants at m/z: 69 for $[C_4H_4O]H^+$ and 73 for $[C_4H_8O]H^+$ using the $[H_3O]^+$ precursor ion. Results obtained using $[O_2]^+$ and $[NO]^+$ as the precursor ion led to identical kinetic results, but with lower sensitivity and were not used in the final kinetic analysis. In the measurements with isoprene and *n*-butanol as the reference compound, FTIR was the only detection method used. The FTIR system recorded absorption spectra at discrete reaction times, that is, at furan and reference compound losses of ~5%–10% per measurement. FTIR spectra were recorded with 64 co-added scans at 1 cm^{-1} resolution. Spectral analysis used the furan infrared spectrum measured in this work and reference spectra for *n*-butanol,[26] THF,[26] and isoprene,[27] available in the literature.

2.2 | Photochemical reactor (PCR) relative rate measurements

The PCR apparatus consists of four major components: (i) a 90 cm long cylindrical double-wall glass gas flow reactor equipped with quartz windows. The reactor temperature was maintained by circulating temperature regulated water through the reactor jacket; (ii) a 16.3 cm long single-pass Pyrex absorption cell with KBr windows mounted in the FTIR sample compartment; (iii) a Teflon pump to circulate the gas mixture between the reactor and absorption cell; and (iv) a Nd:YAG pulsed laser (3rd harmonic: 355 nm, 1–10 Hz) photolysis light source.

OH radicals were produced by the 355 nm pulsed laser photolysis of HONO:

$$HONO + h\nu \rightarrow OH + NO \quad (5)$$

HONO was synthesized online and transferred into the reactor by flowing N_2 bath gas over the headspace of a $H_2SO_4/NaNO_2$ solution (see materials section). The reactor pressure increased ~70 Torr (660–730 Torr) over the duration of an experiment.

k_1(296 K) was measured at a nominal 700 Torr (syn. air) with OH + $CHF{=}CF_2$[28] as the reference reaction, $k(296\ K) = 0.82 \times 10^{-11}$ cm^3 $molecule^{-1}$ s^{-1}.[28] Infrared absorption cross sections for $CHF{=}CF_2$ was taken from the literature.[28]

2.3 | Furan infrared spectrum

Infrared absorption cross sections were measured using FTIR spectroscopy and static gas fills of an absorption cell of 16.3 cm pathlength (PCR, UoC). Spectra were recorded at 1 cm^{-1} resolution between 400 and 4000 cm^{-1} in 128 co-added scans. C_4H_4O was introduced into the absorption cell either as a pure compound or from a mixture in He (13.6% and 16.6%). Independent measurements were made with C_4H_4O concentrations in the range (0.50–6.25) $\times 10^{17}$ molecule cm^{-3}. At least eight different furan concentrations were used in each set of cross section determinations. The furan Beer-Lambert analysis is shown in Figure S1. The agreement between the individual determinations was excellent, to within 2%. A digitized furan infrared

absorption spectrum is given in the supplement in JCAMP-DX format.

2.4 | Computational methods

The thermochemistry for OH radical addition to the two chemically different carbons of C_4H_4O double bonds as well as the direct abstraction pathways were investigated using quantum mechanical molecular calculations and the *Gaussian*16 program suite. C_4H_4O, H_2O, dehydrogenated radicals and the possible OH-furan adduct geometries and frequencies were calculated at the MP2/6-31+G(3df,2p) level of theory, while absolute electronic energies were finely adjusted employing the CCSD(full) method in conjunction with TZVP basis set. The optimized geometries were verified to correspond to global minima by the lack of any negative frequency values. The uncertainty in thermochemistry calculations is estimated to be less than 5 kJ mol^{-1} for the studied reactions.[16] Yuan et al.[29] have previously theoretically studied the kinetics and the reaction mechanism for reaction 1. In our thermochemical approach the reaction pathways enthalpy, entropy and free energy, ΔH, ΔS and ΔG, were calculated as a function of temperature to evaluate the OH-furan adduct thermodynamic stability over the temperature range of the present kinetic measurements and determine that our measured k_1(T) values correspond to the forward rate coefficient. A comparison between temperature dependence ΔG of association and H-atom abstraction channels is also presented.

2.5 | Materials

All reactants, besides HONO, were obtained commercially: C_4H_4O (Sigma–Aldrich, 99%, 0.025 wt% butylated hydroxytoluene as an inhibitor), C_4H_8O (Sigma–Aldrich, ≥ 99.9%), C_5H_8 (Sigma–Aldrich, 99%, < 1000 ppm p-tert-butylcatechol as an inhibitor), n-$CH_3(CH_2)_2CH_2OH$ (Sigma–Aldrich, ≥ 99.7%), $CHF{=}CF_2$ (Synquest Labs, 98%), and He (Linde, 99.996%). Reactants were degassed several times through freeze-pump-thaw cycles at 77 K prior to their storage in darkened Pyrex bulbs. Dilute furan mixtures were manometrically prepared via furan condensation at 77 K and turbulent mixing with He, at room temperature, in a 10 L bulb. The mixing ratio of the prepared mixtures were also calibrated by flow-calibration experiments using pure C_4H_4O, as reference, and quadrupole mass spectrometry detection. The results of the two different techniques were in excellent agreement, to within 1%, verifying the accuracy of the C_4H_4O concentration used in the infrared spectrum measurements. HONO was synthesized online by adding 0.1 M aqueous $NaNO_2$ dropwise (~0.5 mL min^{-1}) into ~50 mL of 0.5 or 1 M aqueous solution of H_2SO_4.[16] NO_2 impurity levels were continuously monitored via FTIR. Pressure was measured by 100 and 1000 Torr calibrated pressure sensors.

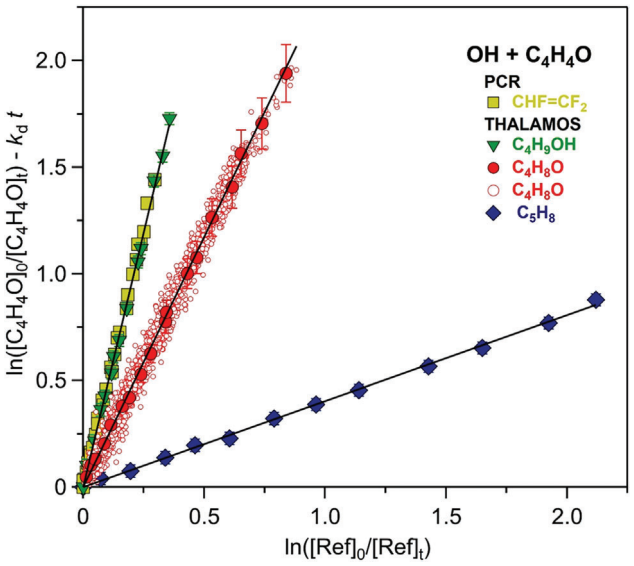

FIGURE 1 Relative rate plot for the OH radical reaction with furan at 296 K obtained for the different reference reactions used (see legend). Data include rate coefficient measurements obtained with both THALAMOS (296 K, 760 Torr syn. air) and PCR (296 K, 700 Torr syn. air) apparatuse (see legend). Red solid and open symbols denote data obtained with FTIR and SIFT-MS detection methods, respectively.

3 | RESULTS AND DISCUSSION

Results for the independent k_1(273–353 K) and k_1(296 K) measurements are presented below. The kinetic results are then compared with the available literature kinetic data and discrepancies discussed.

Table 1 summarizes the experimental conditions and the results obtained for k_1(T). Figure 1 shows results from typical relative rate kinetic experiments at 296 K and 700 and 760 Torr, for the four different reference reactions used in this study. Experiments performed at temperatures other than 296 K were of similar quality and are displayed in Figures S2–S4. k_1(296 K) obtained using the THALAMOS and PCR setups, which used different OH radical sources and reference compounds, are in excellent agreement, to within 5%. The final value for k_1(296 K) was obtained from an average of the individual measurements to be $(4.07 \pm 0.05) \times 10^{-11}$ cm^3 molecule^{-1} s^{-1}. k_1(T) was determined using at least two different reference reactions at each temperature resulting in values that agreed to better

TABLE 1 Summary of the experimental conditions and the kinetic results, k_1(T), for the gas phase OH + C_4H_4O reaction obtained with both PCR and THALAMOS techniques.

T (K)	Ref	$[C_4H_4O]_0$[a]	$[Ref]_0$[a]	$[H_2O_2]_0$[a]	Measured k_1/k_{Ref}[b] FTIR[c,d]	Measured k_1/k_{Ref}[b] SIFT-MS[c,e]	k_1[c] (10^{-11} cm^3 molecule^{-1} s^{-1})
273	C_5H_8	13.8	6.9	24.6	0.40 ± 0.01		4.48 ± 0.08
	C_4H_8O	0.3	0.22	0.58		2.37 ± 0.03	4.39 ± 0.02
		29.3	10.5	34.3	2.44 ± 0.04		4.51 ± 0.02
							$k_{1,avg}$(273 K) = (4.45 ± 0.04)[f]
296	C_5H_8	6.5	7.9	14.7	0.40 ± 0.01		4.04 ± 0.05
	C_4H_8O	0.25	0.15	0.49		2.43 ± 0.02	4.28 ± 0.01
		10.3	7.02	10.6	2.32 ± 0.04		4.08 ± 0.05
		0.61	0.47	1.06		2.27 ± 0.04	4.00 ± 0.02
	C_4H_9OH	5.16	24.3	29.5	4.77 ± 0.07		4.05 ± 0.04
	$CHF=CF_2$[g]	900	320		4.87 ± 0.10		3.99 ± 0.03
		960	412		4.91 ± 0.10		4.03 ± 0.03
							$k_{1,avg}$(296 K) = (4.07 ± 0.05)[f]
323	C_5H_8	12.8	7.4	16.2	0.40 ± 0.01		3.66 ± 0.09
	C_4H_8O	0.29	0.20	0.46		2.19 ± 0.01	3.67 ± 0.02
		22.6	14.2	11.0	2.17 ± 0.05		3.64 ± 0.02
							$k_{1,avg}$(323 K) = (3.66 ± 0.03)[f]
353	C_5H_8	8.6	7.9	19.3	0.40 ± 0.01		3.32 ± 0.08
	C_4H_8O	0.36	0.25	0.41		2.17 ± 0.02	3.47 ± 0.02
		38.7	28.2	12.8	2.05 ± 0.04		3.28 ± 0.01
							$k_{1,avg}$(353 K) = (3.38 ± 0.06)[f]

Note: Experiments carried out between 273 and 353 K at 700 and 760 Torr (syn. Air).

[a]Concentrations in units of 10^{14} molecule cm^{-3}.

[b]Furan dark and photolysis loss corrections have been applied in the relative rate ratio using expression 3. K_d was measured prior to each measurement and was in the range (1–1.5) × 10^{-5} s^{-1} and k'_d was zero in all cases.

[c]Uncertainties are the 2σ precision from the fits.

[d]$k_1/k_{Ref,}$ ratio measured using FTIR detection.

[e]k_1/k_{Ref} ratio measured using SIFT-MS detection.

[f]Averaged k_1(T) values from different references and detection methods used, at each temperature.

[g]Experiments carried out in PCR with 355 nm photolysis of HONO as OH radicals precursor.

than 7% (see Table 1). k_1(T), shown in Figure 2, displayed a negative temperature dependence that is very well represented by the Arrhenius expression $(1.30 \pm 0.08) \times 10^{-11}$ exp[(336 ± 20)/T] cm^3 molecule^{-1} s^{-1}. The quoted uncertainties are the 2σ precision from the fit. Including an estimated 7% systematic error from the reference reaction rate coefficients in a root mean square error analysis yields $k_1(T) = (1.30 \pm 0.12) \times 10^{-11}$ exp[(336 ± 20)/T] cm^3 molecule^{-1} s^{-1}.

In the present work, an emphasis was placed on an evaluation of systematic errors and measurement reproducibility. Experimental condition variations were used as a diagnostic to minimize measurement artefacts and improve measurement precision and accuracy. In particular, k_1(296 K) determinations were carried out in two independent apparatuses that have substantially different configurations. Besides the different reactors, PCR experiments used monochromatic laser light, 355 nm, as the HONO photolysis source of OH radicals. In the THALAMOS experiments, OH radicals were produced by broad band, UV-C lamps, H_2O_2 photolysis. In addition, the reactant concentrations in the PCR experiments were ~2 orders of magnitude greater than used in the THALAMOS experiments. Even given these differences, agreement in k_1 was better than 7%. This demonstrates the high level of reproducibility and precision (repeatability), ~2%, of our measurements and that potential furan secondary chemistry was negligible. In addition, the use of four different reference reactions allowed to evaluate and minimize systematic uncertainties associated with the selection of the reference rate coefficient in this study. In all cases, the k_1 agreement was better than 7%, which also implies that the reference reaction rate coefficients are better known than their quoted uncertainties in the literature. The overall consistency of the measured rate coefficients obtained with four different reference compounds, that is, the high

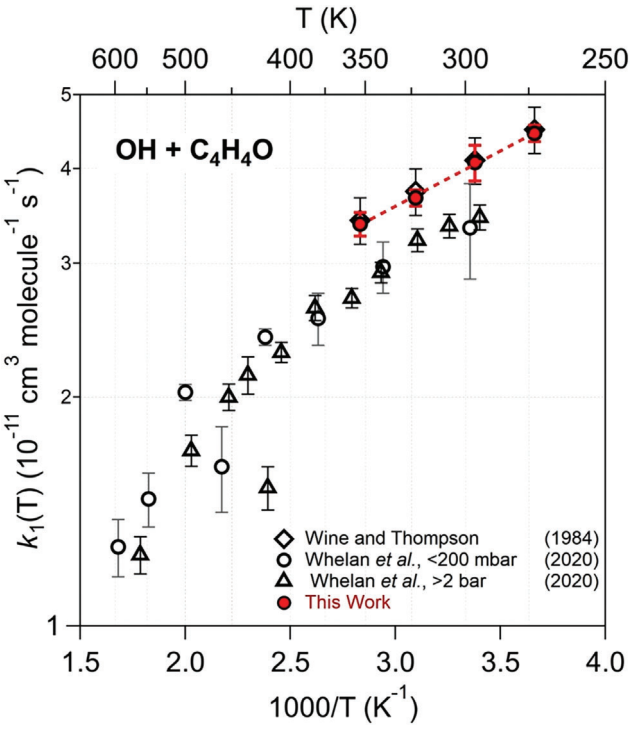

FIGURE 2 Arrhenius plot comparing all the temperature dependent rate coefficient values available in the literature. This work data are shown with solid red circles. Error bars are the 2σ precision from the RR data fits and encompass multiple determination variations. The red dashed line is a least-square fit of the present data to an Arrhenius expression ($k_1(T) = (1.30 \pm 0.08) \times 10^{-11}$ exp[$(336 \pm 20)/T$] cm^3 molecule^{-1} s^{-1}). Temperature dependent rate coefficient data from Wine and Thompson[12] and Whelan et al.[11] are included for comparison (see legend).

level of repeatability and reproducibility of our measurements (see Table 1), provides additional confidence in the present results.

3.1 | Comparison with literature data

There are several room temperature absolute and relative rate measurements of k_1 in the literature to compare with the present results (Table 2).[6–12] There are two determinations of the temperature dependence of k_1,[11,12] that applied absolute rate (AR) methods. The pressure dependence of $k_1(T)$ has been evaluated in several studies, which has shown $k_1(T)$ to be pressure independent over the pressure range 0.005–10 bar and temperature range 294–595 K. Therefore, all $k_1(T)$ values, currently available in the literature were obtained in the reactions high-pressure limit.

Although the differences between the present measurement of $k_1(T)$ and previous results is not large, it is worthwhile to consider the potential systematic errors in both absolute and relative rate kinetic measurement methods. AR and RR methods are susceptible to different potential sources of systematic error of different origin, for example, absolute concentration determination, sample purity, secondary radical chemistry, heterogeneous loss, etc. Here, we will briefly discuss the major sources of systematic error and how they were addressed in the present study.

A key element in kinetic measurements is the determination of the reactant sample concentration and purity. Particularly in AR kinetic measurements, it is critical to know the reactant absolute concentration inside the reactor, while it is not necessary in RR measurements. In some cases, this can be the primary source of uncertainty in an AR measured rate coefficient and can result in either overestimates or underestimates of the reaction rate coefficient. Another important consideration in AR measurements, but less so in RR measurements, is the presence of reactive sample impurities, which would result in an overestimate of the rate coefficient. This does not appear to be an issue in the comparison of the OH + furan studies. A major unavoidable source of uncertainty in RR measurements is the reference reaction rate coefficient uncertainty. Few compounds have rate coefficients known to better than 5%–10%. The present study addressed this potential source of uncertainty by performing independent experiments with multiple reference compounds. In addition, secondary radical chemistry is also a potential source of error in both AR and RR measurements. OH radical regeneration can lead to lower OH rate coefficients in AR measurements, while the formation of other radical species could affect RR measurements. In the present work, different OH radical precursors and photolysis sources as well as different reference compounds were used to experimentally demonstrate that secondary chemistry did not influence the determination of $k_1(T)$.

Table 2 and Figure 3 compare $k_1(296\ K)$ measured in this work with the available literature data. Lee and Tang[6] reported a value of $k_1(296\ K)$ using a Flash Photolysis/Resonance Fluorescence technique (FP/RF) technique. Their $k_1(296\ K)$ value is, however, an outlier, a factor of ~3 greater than all the other measurements and has not been included in Figure 3, or considered further. Atkinson et al.,[7] Tuazon et al.,[8,9] and Bierbach et al.[10] measured $k_1(296\ K)$ using RR methods and reported values of $(3.93 \pm 0.28) \times 10^{-11}$, $(3.98 \pm 0.35) \times 10^{-11}$, and $(4.19 \pm 0.21) \times 10^{-11}$ cm^3 molecule^{-1} s^{-1}, respectively, with the error limits representing the 2σ precision of the RR data fits. In the Atkinson et al.[7] determination OH + *n*-hexane was used as the reference reaction, $k(298\ K) = 5.58 \times 10^{-11}$ cm^3 molecule^{-1} s^{-1}.[9] There are several room temperature rate coefficients values for the OH + *n*-hexane reaction in

TABLE 2 Comparison of OH + C_4H_4O reaction room temperature rate coefficients, k_1(296 K), data available in the literature.

Reference	Experimental technique	Temperature (K)	Total pressure (mbar)	k_1(296 K)[a] (10^{-11} cm^3 molecule^{-1} s^{-1})
Lee and Tang[6]	DF-RF	295	2.17–3.39	1.05 ± 0.08
Atkinson et al.[7]	RR/GC-FID	298	980	3.75 ± 0.28
Tuazon et al.[8]	RR/GC-FID	295	980	4.23 ± 0.32
Bierbach et al.[10]	RR/GC-FID	300	1013	4.19 ± 0.21
Wine and Thompson[12]	PF-RF	254–425	40–200	4.04 ± 0.61[b]
Whelan et al.[11]	PLP-LIF	294–560 298–595	(2–10) × 10^3 5–200	3.45 ± 0.13 3.34 ± 0.48
This work	RR/SIFT-MS RR/FTIR	273–353	1013	4.07 ± 0.05 4.07 ± 0.22[b]

Abbreviations: DF-RF, discharge flow – resonance fluorescence; PF-RF, pulsed photolysis – resonance fluorescence; PLP-LIF, pulsed laser photolysis – laser induced fluorescence; RR/SIFT-MS, relative rate/selected ion flow tube-mass spectrometry; RR/GC-FID, relative rate/gas chromatography – flame ionization detection; RR/FTIR, relative rate/Fourier transform infrared.

[a]The uncertainties are the 2σ precision of the fits.

[b]Uncertainties include differences in independent measurements.

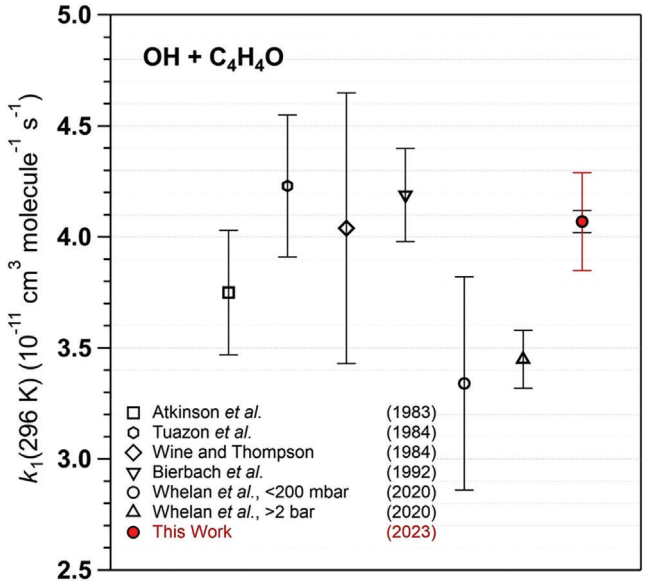

FIGURE 3 k_1(296 K) comparison between this work and the available literature data (see legend). The present uncertainties of all the literature values are the 2σ precision from the fits. This work k_1(296 K) is presented with dual error limits with the 2σ measurement precision shown in black and the differences in the independent measurements are presented in red.

the literature.[7,30–36] k(296 K) values vary between 5.00 and 5.70 × 10^{-11} cm^3 molecule^{-1} s^{-1} with an average k(296 K) = 5.33 × 10^{-11} cm^3 molecule^{-1} s^{-1}. The Atkinson et al.[7] k(296 K) value reported in Table 2 and Figure 3 has been revised based on the average k(296 K) value for the OH radical + *n*-hexane reaction. Tuazon et al.[8] used a RR method with OH + 2-methyl-1,3-butadiene (isoprene, k(298 K) = 9.60 × 10^{-11} cm^3 molecule^{-1} s^{-1}) as the reference reaction. k_1(296 K) included in Table 2 and Figure 3 has been revised using the current recommendation for OH + CH_2=C(CH_3)CH=CH_2 reaction (isoprene, k(298 K) = 1.02 × 10^{-10} cm^3 molecule^{-1} s^{-1}),[23] leading to a ~6% higher absolute rate coefficient value. In the Bierbach et al.[10] RR measurements, OH + CH_2=$CHCH_3$ (propene, k(296 K) = 2.60 × 10^{-11} cm^3 molecule^{-1} s^{-1}) was used as reference reaction, which agrees with the current rate coefficient recommendation.[23] The Bierbach et al.[10] measurement included significant corrections attributed to furan photolysis, up to 25%, although the UVA-Visible photolysis lamps (Philips TL05/40 W: 320–480 nm, λ_{max} = 365 nm) used to photolyze CH_3ONO and produce OH radicals, would not photolyze furan (see furan UV absorption spectrum given in MPI-Mainz UV/VIS Spectral Database[37]). No background or photolysis corrections were employed in the Atkinson et al.[7] and Tuazon et al.[8,9] studies. Error bars shown in Figure 2, for the relative rate studies, are the 2σ fit precision obtained in experiments with a single reference compound.

Wine and Thompson,[12] in their absolute rate measurements, used pulsed photolysis of H_2O (165–185 nm) to produce OH radicals, that also leads to H atom formation in a 1:1 yield, and resonance fluorescence to detect it. H atoms could possibly react with C_4H_4O, but since furan was in large excess to ensure pseudo-first order conditions in OH (initial [OH] ~1 × 10^{11} molecule cm^{-3}), it would not affect the furan concentration and thus the second-order rate coefficient measured. The authors reported a rate coefficient of (4.04 ± 0.61) × 10^{-11} cm^3 molecule^{-1} s^{-1}, with a 2σ uncertainty, that includes fit precision and measurement variability, but not possible systematic uncertainties. Their quoted error limits are three times greater than our quoted uncertainty mainly due to the scatter in their k_1(296 K) determinations.

Whelan et al.[11] using laser pulsed photolysis to form OH radicals and laser induced fluorescence to detect it. They reported low pressure, < 200 mbar, and high pressure, > 2 bar, k_1(294 K) values of $(3.34 \pm 0.48) \times 10^{-11}$ and $(3.45 \pm 0.13) \times 10^{-11}$ cm^3 molecule^{-1} s^{-1}, respectively, with their reported uncertainties given as 2σ (unknown origin).

Our reported room temperature value is also presented in Figure 3, with two different error bars; the black error bar represents the 2σ precision of the measurements, while the red includes differences in the independent measurements. Comparing the quoted error limits of our k_1 values with those of the other measurements, the precision of the present results is substantially higher, ~2%, and 4–6 times less than the error limits reported in all the other studies. Note that the precision obtained for the different reference compounds is nearly identical. The agreement between our k_1(296 K) value and the absolute room temperature rate coefficients from all the previous studies is better than 4%, while the Atkinson et al.[7] revised k_1(296 K) is still in reasonable agreement, ~8% lower. However, the Whelan et al.[11] k_1(296 K) value is substantially lower, ~15%, and falls outside the error limit margins even for the measurements at < 200 mbar that have rather large error limits.

Whelan et al.[11] attributed their substantially smaller room temperature rate coefficient values, ~10%–25%, to possible systematic errors in the previous studies due to secondary chemistry initiated by the OH precursors and photolysis wavelengths used. However, the results from our study, which were performed with various background loss tests, different OH precursors, and photolysis sources contradict this supposition.

The measured temperature dependence of k_1 determined in this work can be compared with results from the Wine and Thomson[12] and Whelan et al.[11] studies. Their k_1(T) data are included in Figure 2 for comparison with the present work. Wine and Thompson[12] studied the OH kinetics between 254 and 425 K, while the Whelan et al.[11] measurements from 294 to 595 K. The results from the present study are in excellent agreement with the results from the Wine and Thompson.[12] The Whelan et al.[11] k_1(T) data are systematically lower by ~15%–20% than the present results, and those of Wine and Thompson,[12] over the 273–425 K temperature range. In all three temperature dependent kinetics studies, a negative temperature dependence was observed. Besides the systematic difference between this work and Whelan et al.[11] k_1(T) values, the activation energies are essentially the same, in the overlapped temperature range, with the Whelan et al.[11] E/R value to be $-(375 \pm 86)$ K, combining low and high pressure data, and ours $-(336 \pm 20)$ K. The corresponding pre-exponential factor in Whelan et al.[11] work was $(9.74 \pm 0.26) \times 10^{-12}$ cm^3 molecule^{-1} s^{-1}, for this temperature range, that is ~25% lower compared to the results from this work. Figure 4 shows all the temperature dependent data available in the literature after scaling the Whelan et al.[11] and Wine and Thomson[12] data to the k_1(296 K) value measured in this work.

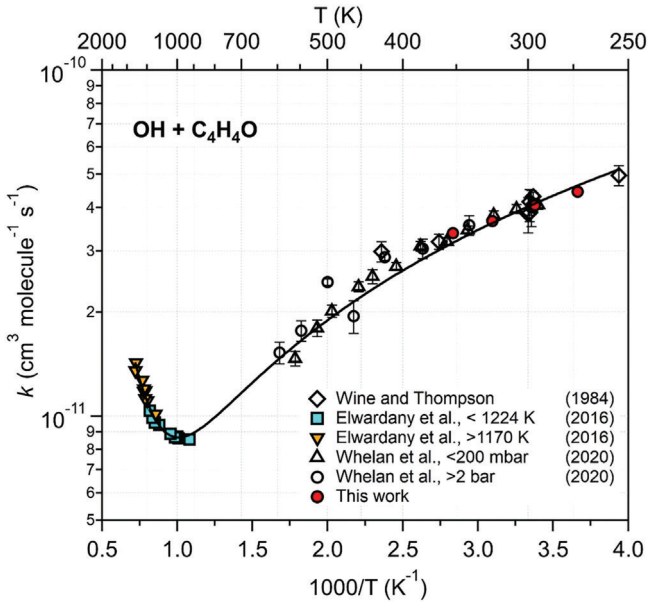

FIGURE 4 Arrhenius plot that includes the temperature dependent measurements available in the literature (see legend). Wine and Thompson,[12] and Whelan et al.[11] data have been scaled to the k_1(296 K) value measured in this work. The solid line is a fit of all the data to the expression $k_1(T) = A_1 \times (T/300)^b + A_2 \times (T/1000)^c \times \exp[-(E/RT)]$ originally presented in the Whelan et al.[11] analysis.

Whelan et al.[11] rationalized their kinetic measurements using MESMER[38] simulations, with input files developed by Yuan et al.[29] The analysis combined their data with the high temperature rate coefficients obtained in the shock-tube study of Elwardany et al.[39] The MESMER analysis does not address the high-temperature abstraction reaction and that pathway was included as a $A(T/300)^n$ dependence. The simulation yielded the expression $k_1(T) = 3.5 \times 10^{-11} (T/300)^{-1.61} + 9.5 \times 10^{-11} (T/1000)^{-0.44} \exp[-(25.6 \text{ kJ mol}^{-1}/RT)]$ cm^3 molecule^{-1} s^{-1}. Here, we have scaled the Wine and Thompson[12] and Whelan et al.[11] data to our more precise room temperature k_1 value, as shown in Figure 4. A fit of the scaled data using the same expression yields $k_1(T) = 4.03 \times 10^{-11} (T/300)^{-1.48} + 5.83 \times 10^{-11} (T/1000)^{+2.18} \exp[-(28.4 \text{ kJ mol}^{-1}/RT)]$ cm^3 molecule^{-1} s^{-1}, that reproduces the experimental data very well with a reasonably acceptable different set of parameters than given in Whelan et al.[11] (see Figure 4).

The dip of the curve between 700 and 1000 K and the positive temperature dependence at higher temperatures is consistent with the transition from an adduct formation reaction mechanism at lower temperatures and a

H-abstraction mechanism at higher temperatures. That is, the OH-furan adduct becomes gradually less stable and the H-abstraction reaction channels becomes significant with temperature increase. This is consistent with our free energy thermochemical calculations, which show that OH addition to the α-carbon (Figure S5) becomes endoergic, $\Delta G > 0$, at ~870 K, Figure S6. The reaction mechanism pathway competition results in the observed valley in the Arrhenius curve. When the OH-furan adduct, which is formed due to the OH radical association to the furan double bond, is no longer stable, the H atom abstraction channel becomes the dominant reaction pathway leading to positive temperature dependence in k_1(T).

Yuan et al.[29] suggest that the OH association proceeds via a van-der Waals pre-reactive complex formation resulting in an excited OH-furan adduct, which further can either be thermally stabilized and yield cyclic oxidation products, such as maleic anhydride ($C_4H_2O_3$), or via ring-opening to form predominately (*E*)- and (*Z*)-butenedial ($C_4H_4O_2$). Bierbach et al.[40] measured a total yield of the two butenedial conformers > 0.70, in the absence of NO_x, while Gómez Alvarez et al.,[41] and Aschmann et al.[42] reported unity and 0.75 molar yields, respectively.

In both THALAMOS and PCR experiments, $C_4H_2O_3$ was detected as a OH + furan reaction product by both SIFT-MS and FTIR. The determination of the maleic anhydride reaction yield in the present and previous studies is complicated by its wall-loss, UV photolysis, and reaction with the OH radical, $k(296\ \text{K}) = (3.93 \pm 0.28) \times 10^{-13}$ cm^3 molecule^{-1} s^{-1}.[43] There was evidence of $C_4H_2O_3$ loss in the PCR measurements at higher furan conversion, that is, downward curvature in the product yield plot was observed. Curvature was not observed in the THALAMOS experiments (see Figure S7). We attribute this difference to $C_4H_2O_3$ wall-loss, which would be less in the ~2.5 times lower surface-to-volume ratio of the THALAMOS apparatus. The linear fit of the PCR data in the furan conversion region resulted in a maleic anhydride yield of (1.27 ± 0.05)%. The maleic anhydride yield in the THALAMOS experiments was slightly greater at (3.15 ± 0.20)%. We report a 3% maleic anhydride yield as a lower-limit due to possible unaccounted for losses of $C_4H_2O_3$ in the THALAMOS experiments. The detection of maleic anhydride as a reaction product provides evidence that a minor OH + furan reaction pathway does not lead to furan ring opening.

3.2 | Atmospheric implications

The furan atmospheric lifetime due to OH reactive loss, τ(OH), using $k_1(273\ \text{K}) = 4.45 \times 10^{-11}$ cm^3 molecule^{-1} s^{-1} from this work and a globally averaged OH concentration of 10^6 molecule cm^{-3}, was estimated to be 6.2 h.

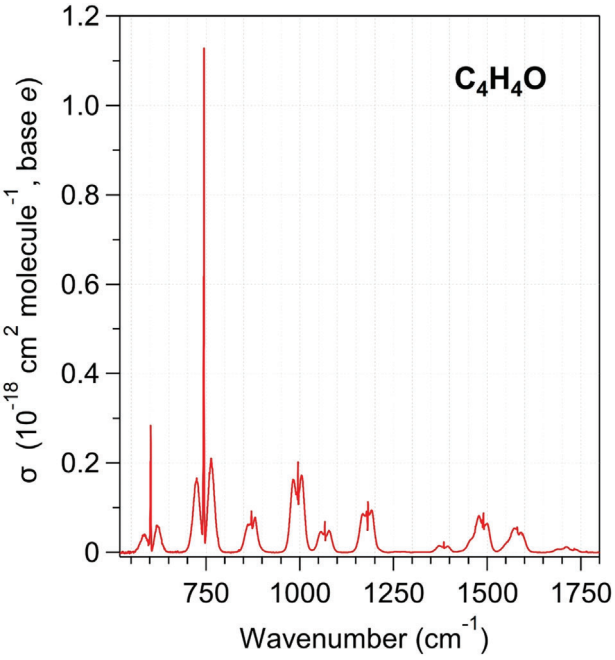

FIGURE 5 Infrared gas-phase absorption spectrum of furan (C_4H_4O). Spectra were recorded at 1 cm^{-1} resolution in a 16.3 cm single pass absorption cell with static furan concentrations between 0.50 and 6.25×10^{17} molecule cm^{-3}. Cross section was determined from a Beers law analysis (see Figure S1). The integrated band strength (IBS) over the 520–1800 cm^{-1} region was determined to be $(3.51 \pm 0.03) \times 10^{-17}$ cm^2 molecule^{-1} cm^{-1}. A digitized spectrum is provided in the SI.

Newland et al.[44] and Al Ali et al.[45] have reported room temperature rate coefficients for the NO_3 radical + C_4H_4O reaction to be $(1.49 \pm 0.23) \times 10^{-12}$ and $(1.51 \pm 0.38) \times 10^{-12}$ cm^3 molecule^{-1} s^{-1}, respectively. They estimated daytime and nighttime furan lifetimes, $\tau(NO_3)$, of 19 and ~1 h, respectively, for NO_3 reactive loss using 1×10^7 (daytime) and 2×10^8 (nighttime) molecule cm^{-3} NO_3 radical concentrations. In addition, Atkinson et al.[7] and Andersen et al.[46] have reported furan atmospheric lifetime with respect the reaction with O_3 to be 119 h. Thus, O_3 chemistry is expected to be a minor atmospheric removal process for furan. The OH radical reaction is expected to dominate the daytime loss of furan, while reaction with the NO_3 radical is expected to be the predominant nighttime loss process.

On the basis of the τ(OH) estimated in this work and the measured infrared spectrum (Figure 5), the furan well mixed (instantaneous) and lifetime adjusted radiative efficiencies were calculated to be 0.058 and $\sim 5 \times 10^{-4}$ W m^{-2} ppb^{-1}, respectively.[47] A 20-year time horizon global warming potential, GWP_{20}, of $\sim 5 \times 10^{-5}$ is estimated using the adjusted RE. (Figure S8).

The furan infrared spectrum measured in this work (1 cm^{-1} resolution) can be compared with the high-resolution infrared spectrum reported in the PNNL database.[26] The PNNL infrared spectrum was recorded between 550 and 6500 cm^{-1}, at 0.112 cm^{-1} resolution. Due to the different resolution of the spectra, we are comparing the integrated band strengths (IBS) for bands in the range 500–1800 cm^{-1}. The IBSs for the furan bands between 810 and 1800 cm^{-1} are in excellent agreement, within 0.5%–3%. However, significant differences were observed for the bands centered at 602 and 744 cm^{-1}, with the IBS values measured in this work being 35 and 40% smaller, respectively. This may imply that the 7th order polynomial baseline correction applied in the PNNL spectrum may have led to overestimating these absorption features. The observed discrepancy affects the furan RE by ~20%.

4 | CONCLUSIONS

Rate coefficients, k_1, for the gas-phase OH radical + furan (C_4H_4O) reaction were determined as a function of temperature between 273 and 353 K, using two independent apparatuses employing RR methods. The results from this study are consistent with the previous work by Wine and Thompson[12] and systematically greater by ~15%–20% compared to the more recent study by Whelan et al.[11] The negative temperature dependence for the OH + furan reaction is consistent with a complex reaction mechanism that predominately proceeds via OH radical association to furan's double bonds, at atmospherically relevant temperatures and pressures. Thermochemical molecular calculations showed that although both OH radical association channels to the two chemically different carbons of furan are exothermic, −121.5 (α-carbon with respect the ether-group) and −52.9 kJ mol^{-1} (β-carbon), the addition to the α-carbon is thermodynamically preferred. H-atom abstraction from both α- and β-carbons are highly endothermic by 41.9 and 42.3 kJ mol^{-1}, respectively, and it is expected to have negligible contribution under atmospheric degradation conditions. Maleic anhydride ($C_4H_4O_3$) was observed as a minor product (3% yield lower-limit) of the OH + furan reaction, identifying an atmospheric source of maleic anhydride in wildfire plume chemistry.

ACKNOWLEDGMENTS

This work was supported in part by the NOAA Climate Goal and NASA Atmospheric Composition Programs. MEA was co-funded by Greece and the European Union (European Social Fund – ESF) through the Operational Programme «Human Resources Development, Education and Lifelong Learning» in the context of the project "Strengthening Human Resources Research Potential via Doctorate Research" (MIS-5000432), implemented by the State Scholarships Foundation (IKY) and the Erasmus+ programme of the European Union for visiting IMT Nord Europe institute. This work is part of the CaPPA project funded by the ANR through the PIA under contract ANR-11-LABX-0005-01, and the CPER ECRIN project, funded by the Hauts-de-France Regional Council. This work was also supported by the French National program LEFE (Les Enveloppes Fluides et l'Environnement), in the framework of FiLL project. VCP was supported in part by Labex CaPPA, IMT Nord Europe.

CONFLICT OF INTEREST STATEMENT

There is no conflict of interest to disclose.

DATA AVAILABILITY STATEMENT

The data that supports the findings of this study are available in the supplementary material of this article.

ORCID

Manolis N. Romanias https://orcid.org/0000-0002-9049-0319

James B. Burkholder https://orcid.org/0000-0001-9532-6246

Vassileios C. Papadimitriou https://orcid.org/0000-0002-8299-4306

REFERENCES

1. Akagi SK, Yokelson RJ, Wiedinmyer C. Emission factors for open and domestic biomass burning for use in atmospheric models. *Atmos Chem Phys*. 2011;11:4039-4072.
2. Crutzen PJ, Andreae MO. Biomass burning in the tropics: impact on atmospheric chemistry and biogeochemical cycles. *Science*. 1990;250:1669-1678.
3. Naeher LP, Brauer M, Lipsett M. Woodsmoke Health Effects: a Review. *Inhal Toxicol*. 2007;19:67-106.
4. Lim CY, Hagan DH, Coggon MM, et al. Secondary organic aerosol formation from the laboratory oxidation of biomass burning emissions. *Atmos Chem Phys*. 2019;19:12797-12809.
5. Binder JB, Raines RT. Simple chemical transformation of lignocellulosic biomass into furans for fuels and chemicals. *J Am Chem Soc*. 2009;131:1979–1985.
6. Lee JH, Tang IN. Absolute rate constants for the hydroxyl radical reactions with ethane, furan, and thiophene at room temperature. *J Chem Phys*. 1982;77:4459–4463.
7. Atkinson R, Sara M, Carter WPL. Kinetics of the reactions of O_3 and OH radicals with furan and thiophene at 298 ± 2 K. *Int J Chem Kin*. 1983;15:51-61.
8. Tuazon EC, Atkinson R, Winer AM, Pitts JNA. Study of the atmospheric reactions of 1,3-dichloropropene and other selected organochlorine compounds. *Arch Environ Contam Toxicol*. 1984;13:691–700.
9. Atkinson R. Kinetics and mechanisms of the gas-phase reactions of the hydroxyl radical with organic compounds under atmospheric conditions. *Chem Rev*. 1985;85:69-201.

10. Bierbach A, Barnes I, Becker KH. Rate coefficients for the gas-phase reactions of hydroxyl radicals with furan, 2-methylfuran, 2-ethylfuran and 2,5- dimethylfuran at 300 + 2 K. *Atmos Environ*. 1992;26A:813-817.
11. Whelan CA, Eble J, Mir ZS, et al. Kinetics of the reactions of hydroxyl radicals with furan and Its alkylated derivatives 2-methyl furan and 2,5-dimethyl furan. *J Phys Chem A*. 2020;124:7416–7426.
12. Wine PH, Thompson RJ. Kinetics of OH reactions with furan, thiophene, and tetrahydrothiophene. *Int J Chem Kinet*. 1984;16:867–878.
13. Hatch LE, Yokelson RJ, Stockwell CE, et al. Multi-instrument comparison and compilation of non-methane organic gas emissions from biomass burning and implications for smoke-derived secondary organic aerosol precursors. *Atmos Chem Phys*. 2017;17:1471-1489.
14. Warneke C, Roberts JM, Veres P, et al. VOC identification and inter-comparison from laboratory biomass burning using PTR-MS and PIT-MS. *Int J Mass Spectrom*. 2011;303:6-14.
15. Osseiran N, Romanias MN, Gaudion V, et al. Development and validation of a thermally regulated atmospheric simulation chamber (THALAMOS): a versatile tool to simulate atmospheric processes. *J Environ Sci*. 2020;95:141-154.
16. Chattopadhyay A, Bedjanian Y, Romanias MN, et al. OH radical and chlorine atom kinetics of substituted aromatic compounds: 4-chlorobenzotrifluoride (p-$ClC_6H_4CF_3$). *J Phys Chem A*. 2022;126:5407-5419.
17. Romanias MN, Stefanopoulos VG, Papanastasiou DK, Papadimitriou VC, Papagiannakopoulos P. Temperature-dependent rate coefficients and mechanism for the gas-phase reaction of chlorine atoms with acetone. *Int J Chem Kin*. 2010;42:724-734.
18. Papadimitriou VC, Spitieri CS, Papagiannakopoulos P, et al. Atmospheric chemistry of $(CF_3)_2C = CH_2$: oH radicals, Cl atoms and O_3 rate coefficients, oxidation end-products and IR spectra. *Phys Chem Chem Phys*. 2015;17:25607-25620.
19. Zogka AG, Romanias MN, Thevenet F. Formaldehyde and glyoxal measurement deploying a selected ion flow tube mass spectrometer (SIFT-MS). *Atmos Meas Tech*. 2022;15:2001-2019.
20. Papadimitriou VC, Lazarou YG, Talukdar RK, Burkholder JB. Atmospheric chemistry of $CF_3CF = CH_2$ and (Z)-$CF_3CF = CHF$: cl and NO_3 rate coefficients, Cl reaction product yields, and thermochemical calculations. *J Phys Chem A*. 2011;115:167-181.
21. Baasandorj M, Papadimitriou VC, Burkholder JB. Rate coefficients for the gas-phase reaction of (E)- and (Z)-$CF_3CF = CFCF_3$ with the OH radical and Cl-atom. *J Phys Chem A*. 2019;123:5051–5060.
22. Papadimitriou VC, Burkholder JB. OH radical reaction rate coefficients, infrared spectrum, and global warming potential of $(CF_3)_2CFCH = CHF$ (HFO-1438ezy(E)). *J Phys Chem A*. 2016;120:6618–6628.
23. Burkholder JB, Sander SP, Abbatt J, et al. *Chemical kinetics and photochemical data for use in atmospheric studies*. Jet Propulsion Laboratory, Ed. Pasadena; 2019. evaluation No. 19; JPL Publication 19-5.
24. Sime SL, Blitz MA, Seakins PW. Rate coefficients for the reactions of OH with butanols from 298 K to temperatures relevant for low-temperature combustion. *Int J Chem Kinet*. 2020;52:1046-1059.
25. Moriarty J, Sidebottom H, Wenger J, Mellouki A, Le Bras G. Kinetic studies on the reactions of hydroxyl radicals with cyclic ethers and aliphatic diethers. *J Phys Chem A*. 2003;107:1499-1505.
26. Sharpe SW, Johnson TJ, Sams RL, Chu PM, Rhoderick GC, Johnson PA. Gas-phase databases for quantitative infrared spectroscopy. *Appl Spectrosc*. 2004;58:1452–1461.
27. Brauer CS, Blake TA, Guenther AB, Sharpe SW, Sams RL, Johnson TJ. Quantitative infrared absorption cross sections of isoprene for atmospheric measurements. *Atmos Meas Tech*. 2014;7:3839-3847.
28. Baasandorj M, Burkholder JB. Rate coefficient for the gas-phase OH + $CHF = CF_2$ reaction between 212 and 375 K. *Int J Chem Kin*. 2016;48:645-752.
29. Yuan Y, Zhao X, Wang S, Wang L. Atmospheric oxidation of furan and methyl-substituted furans initiated by hydroxyl radicals. *J Phys Chem A*. 2017;121:9306–9319.
30. Behnke W, Holländer W, Koch W, Nolting F, Zetzsch C. A smog chamber for studies of the photochemical degradation of chemicals in the presence of aerosols. *Atmos Environ*. 1988;22:1113-1120.
31. Abbatt JPD, Demerjian KL, Anderson JG. A new approach to free-radical kinetics: radially and axially resolved high-pressure discharge flow with results for hydroxyl + (ethane, propane, n-butane, n-pentane) .fwdarw. products at 297 K. *J Phys Chem*. 1990;94:4566-4575.
32. Donahue NM, Clarke JS, Fitting multiple datasets in kinetics: n-butane + OH → products. *Int J Chem Kinet*. 2004;36:259-272.
33. DeMore WB, Bayes KD. Rate constants for the reactions of hydroxyl radical with several alkanes, cycloalkanes, and dimethyl ether. *J Phys Chem A*. 1999;103:2649-2654.
34. Crawford MA, Dang B, Hoang J, Li Z. Kinetic study of OH radical reaction with n-heptane and n-hexane at 240–340K using the relative rate/discharge flow/mass spectrometry (RR/DF/MS) technique. *Int J Chem Kinet*. 2011;43:489-497.
35. Klein T, Barnes I, Becker KH, Fink EH, Zabel F. Pressure dependence of the rate constants for the reactions of ethene and propene with hydroxyl radicals at 295 K. *J Phys Chem*. 1984;88:5020-5025.
36. Han L, Siekmann F, Zetzsch C. Rate constants for the reaction of OH radicals with hydrocarbons in a smog chamber at low atmospheric temperatures. *Atmosphere*. 2018;9:320-335.
37. Keller-Rudek H, Moortgat GK, Sander R, Sörensen R. The MPI-Mainz UV/VIS spectral atlas of gaseous molecules of atmospheric interest. *Earth Syst Sci Data*. 2013;5:365-373.
38. Glowacki DR, Liang CH, Morley C, Pilling MJ, Robertson SH. MESMER: an open-source master equation solver for multi-energy well reactions. *J Phys Chem A*. 2012;116:9545–9560.
39. Elwardany A, Es-Sebbar E, Khaled F, Farooq AA. Chemical kinetic study of the reaction of hydroxyl with furans. *Fuel*. 2016;166:245–252.
40. Bierbach A, Barnes I, Becker KH. Product and kinetic study of the OH initiated gas-phase oxidation of furan, 2-methylfuran and furanaldehydes at ∼300 K. *Atmos Environ*. 1995;29:2651-2660.
41. Gómez Alvarez E, Borrás E, Viidanoja J, Hjorth J. Unsaturated dicarbonyl products from the OH-initiated photo-oxidation of furan, 2-methylfuran and 3-methylfuran. *Atmos Environ*. 2009;43:1603–1612.

42. Aschmann SM, Nishino N, Arey J, Atkinson R. Products of the OH radical-initiated reactions of furan, 2- and 3-methylfuran, and 2,3- and 2,5-dimethylfuran in the presence of NO. *J Phys Chem A*. 2014;118:457–466.
43. Chattopadhyay A, Papadimitriou VC, Marshall P, Burkholder JB. Temperature-dependent rate coefficients for the gas-phase OH + furan-2,5-dione ($C_4H_2O_3$, maleic anhydride) reaction. *Int J Chem Kinet*. 2020;52:623-631.
44. Newland MJ, Ren Y, McGillen MR, Michelat L, Daële V, Mellouki A. NO_3 chemistry of wildfire emissions: a kinetic study of the gas-phase reactions of furans with the NO_3 radical. *Atmos Chem Phys*. 2022;22:1761-1772.
45. Ali FA, Coeur C, Houzel N, Bouya H, Tomas A, Romanias MN. Rate coefficients for the gas-phase reactions of nitrate radicals with a series of furan compounds. *J Phys Chem A*. 2022;126:8674-8681.
46. Andersen C, Nielsen OJ, Østerstrøm FF, Ausmeel S, Nilsson EJK, Sulbaek Andersen MP. Atmospheric chemistry of tetrahydrofuran, 2-methyltetrahydrofuran, and 2,5-dimethyltetrahydrofuran: kinetics of reactions with chlorine atoms, OD radicals, and ozone. *J Phys Chem A*. 2016;120:7320-7326.
47. Shine KP, Myhre G. The spectral nature of stratospheric temperature adjustment and its application to halocarbon radiative forcing. *J Adv Model Earth Syst*. 2020;12:e2019MS001951.

SUPPORTING INFORMATION

Additional supporting information can be found online in the Supporting Information section at the end of this article.

How to cite this article: Angelaki ME, Romanias MN, Burkholder JB, Papadimitriou VC. Rate coefficients for the gas-phase OH + furan (C_4H_4O) reaction between 273 and 353 K. *Int J Chem Kinet*. 2023;1-12. https://doi.org/10.1002/kin.21697